Results in Physics 12 (2019) 1015–1025

Contents lists available at ScienceDirect

Results in Physics

journal homepage: www.elsevier.com/locate/rinp

Study of main parameters affecting pitting corrosion in a basic medium using the network method

J.F. Sánchez-Pérez[a], F. Alhama[a], J.A. Moreno[b], M. Cánovas[c,*]

[a] Network Simulation Research Group, Department of Applied Physics, Universidad Politécnica de Cartagena (UPCT), Cartagena, Spain
[b] Department of Mechanical Engineering, Universidad Politécnica de Cartagena (UPCT), Cartagena, Spain
[c] Metallurgical and Mining Engineering Department, Universidad Católica del Norte, Antofagasta, Chile

ARTICLE INFO

Keywords:
Pitting corrosion
Prediction
Numerical methods
Reinforced concrete
Steel
Network method

ABSTRACT

This paper presents a mathematical model of pitting corrosion formed by eight non-linear coupled differential equations and their boundary equations. In this model we studied the effect of the variation of parameter values (temperature, crevice depth, oxygen and sodium chloride concentration outside the cavity, and pH) on all the concentrations of the species, and on their differences with their concentrations outside the crevice and along the cavity using the network method. Moreover, a sensitivity study of the system parameters has been carried out. No simplifications have been considered, although the model is firmly coupled and susceptible to any variation of the aforementioned parameters. The development of the model is clearly explained. The results are compared with data published in the scientific literature for domains that establish the most complex and complete scenarios to verify the reliability of the model. One of the practical applications of this work, among others, is focused on the possible effects of this type of corrosion on the reinforced concrete, in buried pipes and on ship hulls.

Introduction

Corrosion generates great economic losses because materials lose their properties and maintenance costs increase [1–3]. Pitting corrosion is one of the most common forms of localized corrosion. Its study is interesting due to the fact that most of the material does not corrode, but remains passive and stable. This type of corrosion occurs on metal parts that are in contact with small volumes of electrolyte solution, such as crevices, pits and surfaces under tension. When the solution enters the crevice or pit, dissolved corrosion products accumulate in the crevice, since the crevice impedes transport away from the metal surface. The resulting change in solution composition somehow leads to the acceleration of corrosion in the crevice or pit [4].

At present, several models are available to predict pitting corrosion, although there is no complete understanding of the mechanisms associated with this type of corrosion [5,6]. Several models have been developed for the study of pitting corrosion [5,6–14]. In literature these models have been classified as empirical, semi-empirical and mechanical. The last models are based on the fundamental processes of pitting corrosion [5,6,10,11].

One of the pursued aims is the practical application of the variables studied. Pitting corrosion alters the properties of the material as it produces small cavities in the iron structure with their consequent tensions. One of the structures which suffers this type of localized corrosion is reinforced concrete. This work focuses on the study of the variables affecting this type of corrosion once it has been initiated by the action of chlorides [15].

Another aim is to design a network model to simulate pitting corrosion, using the rules given by González-Fernández and Alhama [16] to establish the equivalence between the model and the physical processes [17,18]. To simulate the model a circuit analysis software can be used, which uses Spice code, such as PSpice or NgSpice, Microsim Corporation Fairbanks [19], NgSpice software [20] and Nagel [21]. Finally, the spatial discretization of the governing equations is necessary [22–25].

The network method has been used efficiently in several engineering and science problems, such as those related to inverse problems, chemistry, electrochemistry and heat transfer [26–30], as well as in different oxidation problems (CO_2 corrosion -general corrosion-, lubricants degradation, high temperature oxidation and so on) [22–25].

* Corresponding author.
E-mail addresses: juanf.sanchez@upct.es (J.F. Sánchez-Pérez), paco.alhama@upct.es (F. Alhama), josea.moreno@upct.es (J.A. Moreno), manuel.canovas@ucn.cl (M. Cánovas).

https://doi.org/10.1016/j.rinp.2018.12.066
Received 16 October 2018; Received in revised form 7 December 2018; Accepted 17 December 2018
Available online 21 December 2018

Nomenclature

Abbreviations

a_i	parameters and constants
b_i	adjustment coefficients
c	molar concentration of species (M)
C	capacitor, capacitance (F)
CR	corrosion rate (mm/year)
D_j^m	molecular diffusivity (cm^2/s)
E_1, E_2, E_3	controlled voltage-sources
E_{met}	potential at the metal away from the cavity opening (kJ/mol)
F	Faraday's constant (96,487 C/mol)
G_1, G_2, G_3, G_4, G_5	controlled current-sources
i	electric current (A)
I	electric current in the network model (A)
j	electrical current density (A/m^2)
k	reaction rate coefficient ($M^{-1}\ s^{-1}$ or s^{-1})
K	equilibrium constant
K_{perm}	permeability coefficient (cm/s)
M	Molecular mass (g/mol)
n	charge transfer number
q	electric charge (C)
R	universal gas constant (8.314 J/mol·K)
R_j	Resistor (Ω)
t	time (s)
T	temperature (K)
V_1, V_2	batteries (V)
v_j	concentration net rate of the species j (M/s)
x	spatial coordinate (m)
w	pitting width (m)
α	stoichiometric coefficient
μ	dynamic viscosity (kg/ms)
ξ	dielectric constant of water
ρ	density (kg/m^3)
φ	electrostatic potential at the deep of the crack (kJ/mol)
ϕ_j^m	flux associated with the molecular diffusion of each electroactive species (mM/s)

Subscripts

0	initial value
a	anodic
b	backward
C	related to capacitor, critical value
c	cathodic
f	forward
hy	related to hydrolysis of iron II ion
I	generation for chemical reactions
II	net flux term function of first derivate
in	first term of net flux function of second derivate
j	species index
out	second term of net flux function of second derivate
pr	related to precipitation of iron II hydroxide
Ref	reference
w	related to water dissociation

Governing equations

Only the latest models are based on the fundamental processes of pitting corrosion [5,6,10,11]. This type of model broadly describes the electrochemical processes that occur at the metal-liquid interface in the absence of protective films. The effect of these layers would slow down transport and chemical processes in the boundary layer. The chemical environment within a cavity where localized corrosion has occurred is often very different from that produced outside the cavity.

The common goal of mechanistic models is to express the species concentrations in the solution trapped in the cavity as a function of physical and chemical parameters of the system, such as crevice dimensions and composition outside it. Therefore, a complete description of the system should include the complex distribution of the solution

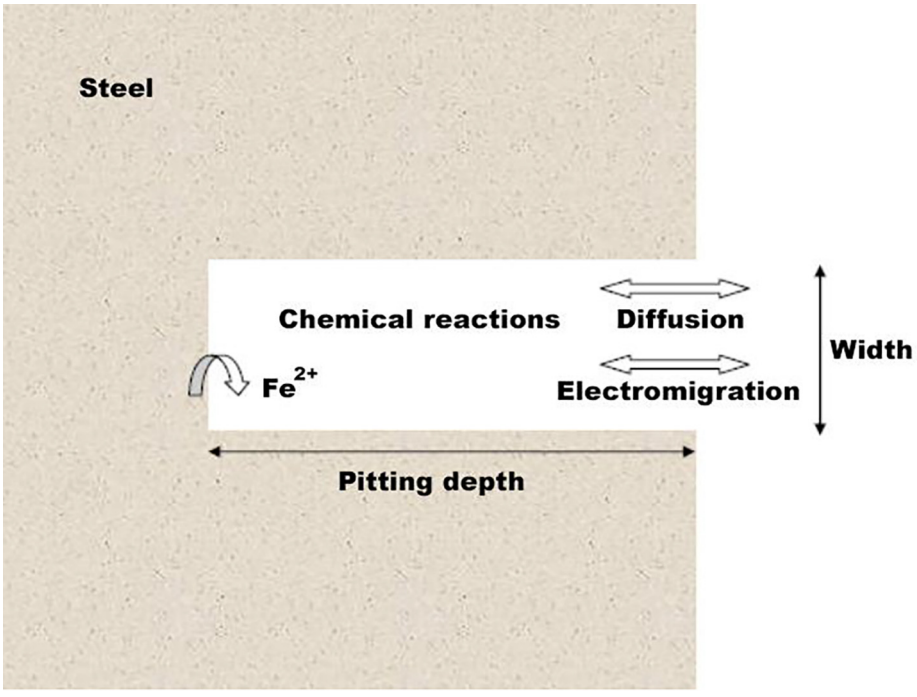

Fig. 1. Scheme of different processes in pitting corrosion.

composition inside the crevice (Fig. 1), rates of electrochemical reactions, ion migration and potential gradients, and the effect of shape and size of the crevice. In turn, the electrochemical reaction rate depends on parameters such as the electrostatic potential and pH solution. Fig. 1 illustrates the different processes that may occur in pitting corrosion.

Corrosion can be subdivided in five different processes: electrochemical reactions, chemical reactions, flux, diffusion and electromigration. Specifically, electrochemical reactions are

- Fe oxidation,
- H^+ reduction,
- Oxygen reduction,
- H_2O reduction

Equations for the reactions above are:

$$Fe \rightarrow Fe^{2+} + 2e^- \tag{1}$$

$$2H^+ + e^- \rightarrow H_2 \tag{2}$$

$$O_2 + 2H_2O + 4e^- \rightarrow 4OH^- \tag{3}$$

$$2H_2O + 2e^- \rightarrow H_2 + OH^- \tag{4}$$

The transfer process is of mixed type. For species where reduction occurs, i. e. cathodic species, the current density, j_c, is given by Eq. (5). For species where oxidation occurs, anodic species, the current density, j_a, is given by Eq. (6).

$$j_c = -j_0\left[e^{\frac{-a_3(E_{met}-\varphi)}{RT}}\right] \tag{5}$$

$$j_a = j_0\left[e^{\frac{a_3(E_{met}-\varphi)}{RT}}\right] \tag{6}$$

$$j_0 = j_{0Ref}\cdot(C_{H+})^{a_1}\cdot(C_{O2})^{a_2} \tag{7}$$

where E_{met} is the potential of the metal far from the cavity opening, R is the universal gas constant, T is the temperature, j_0 and j_{0Ref} are the initial current density and reference current density, respectively, and a_1, a_2 and a_3 are parameters and constants.

The corrosion potential is defined as the electrostatic potential at the deepest point of the crevice, φ. This can be determined from Eq. (8).

$$\sum j_c = \sum j_a \tag{8}$$

Sharland and Tasker [5] and Sharland [6] developed a transport model coupled to an electrochemical model. In their model, electrochemical reactions were boundary conditions.

The resolution of the transport process determines the concentration of these species within the crevice, allowing prediction of iron corrosion.

In the steady state, the flux associated with the molecular diffusion of each electroactive species, ϕ_j^m, runs counter to the concentration gradient direction near the metal-liquid interface and, if it is weak, it may be approximated by the first term of a Taylor series. This expression is Fick's first law, assuming linear dependence [31,32],

$$\phi_j^m = -D_j^m\left(\frac{\partial c_j}{\partial x}\right)_{x=0} \tag{9}$$

where D^m is the molecular diffusion coefficient and c_j the concentration of j species at the interface metal-water.

According to the boundary conditions at the deepest point of the crevice (at the metal surface) Eq. (9) may be opportunely expressed as the rates at which electrons are consumed or emitted in terms of current density, j, i.e.,

$$\phi_j^m = -D_j^m\frac{\partial c_j}{\partial x} = \frac{1}{F}\frac{j_j\alpha_j}{n_j} \tag{10}$$

where α_j is the semi-reaction stoichiometric coefficient, F is Faraday's constant and n_j the charge transfer number. Obviously, the flux of species not involved in the electrochemical reaction and net rates of change within the solution are zero, since they are in equilibrium.

The main chemical reactions that occur include the hydrolysis of iron II ion, precipitation of iron II hydroxide and water dissociation. Equations for these reactions are:

$$Fe^{2+} + H_2O \Leftrightarrow Fe(OH)^+ + H^+ \tag{11}$$

$$Fe(OH)^+ + H_2O \Leftrightarrow Fe(OH)_{2(S)} + H^+ \tag{12}$$

$$H_2O \Leftrightarrow H^+ + OH^- \tag{13}$$

Hydroxide precipitation limits the concentration of iron in the film and in the cavity. The conductivity within the solution can be governed by sodium and chloride ions. Moreover, the solution must include the dissolved oxygen required for the electrochemical reactions.

Net rates of species concentrations' change Fe^{2+} (species 1), $Fe(OH)^+$ (species 2), H^+ (species 5), and OH^- (species 6), can be described in the form

$$\frac{dc_{R,1}}{dt} = -k_{fhy}\cdot c_1 + k_{bhy}\cdot c_2c_5 \tag{14}$$

$$\frac{dc_{R,2}}{dt} = k_{fhy}\cdot c_1 - k_{bhy}\cdot c_2c_5 - k_{fpr}\cdot c_2 + k_{bpr}\cdot c_5 \tag{15}$$

$$\frac{dc_{R,5}}{dt} = k_{fhy}\cdot c_1 - k_{bhy}\cdot c_2c_5 + k_{fpr}\cdot c_2 - k_{bpr}\cdot c_5 + k_{fw} - k_{bw}\cdot c_5c_6 \tag{16}$$

$$\frac{dc_{R,6}}{dt} = +k_{fw} - k_{bw}\cdot c_5c_6 \tag{17}$$

where the subscripts mean: b associated to backward, f related to forward, hy related to hydrolysis of iron II ion, pr associated to precipitation of iron II hydroxide and w related to the water dissociation.

In this corrosion process, chemical reactions inside the cavity occur very quickly and the steady state is reached almost instantaneously, which prevents from obtaining values for the rate constants of reactions (k) 14 to 17. Because the steady state is reached quickly, Eqs. (14)–(17) can be rewritten as a function of the equilibrium constants:

$$\frac{dc_{R,1}}{dt} \approx -K_{hy}\cdot c_1 + c_2c_5 \tag{18}$$

$$\frac{dc_{R,2}}{dt} \approx K_{hy}\cdot c_1 - c_2c_5 - K_{pr}\cdot c_2 + c_5 \tag{19}$$

$$\frac{dc_{R,5}}{dt} \approx K_{hy}\cdot c_1 - c_2c_5 - K_{pr}\cdot c_2 + c_5 + K_w - c_5c_6 \tag{20}$$

$$\frac{dc_{R,6}}{dt} \approx K_w - c_5c_6 \tag{21}$$

where net rates of change in species concentrations, v_j or $\frac{dc_{R,j}}{dt}\Big|_{Chemicalreaction}$, are expressed in terms of the equilibrium constants, K.

Species that do not chemically react, Na^+ (species 3), Cl^- (species 4), and O_2 (species 7), only suffer processes of diffusion and electromigration. Initially, all species in contact with the metal surface are in chemical equilibrium, that is, the net rate of concentration change is zero. Within the solution, initial conditions and boundary conditions are constant.

Concentration variations at the interface, which are governed by the chemical reactions mentioned, must also meet the mass conservation equation, which includes the transport of species. This process can be considered one-dimensional. The equation describing the transport of species j, including the contribution of chemical reactions and the electrostatic potential is [5,6]:

$$\frac{\partial c_j}{\partial t} = wD_j^m\frac{\partial}{\partial x}\left(\frac{\partial c_j}{\partial x} + \frac{nF}{RT}c_j\frac{\partial\varphi}{\partial x}\right) + w\frac{dc_{R,j}}{dt}\Big|_{Chemicalreaction} \tag{22}$$

where x is the spatial coordinate representing the distance from the

edge of the crevice and w is the crevice width. In this equation, the first term represents the accumulation, the second the net flux and the last represents the variation of species j due to chemical reactions.

The molecular diffusion coefficient, D_j^m, can be obtained from Eq. (23). This value approaches the reference value at 25 °C, $D_{j,ref}^m$.

$$D_j^m = \frac{T}{293.15}\cdot\frac{\mu_{ref}}{\mu}\cdot D_{j,ref}^m \tag{23}$$

where μ is the dynamic viscosity.

The electric potential, φ, inside the cavity can be calculated through the following expression [33]:

$$\frac{\partial^2\varphi}{\partial x^2} + \frac{F}{\xi}\sum_j n_j c_j = 0 \tag{24}$$

where ξ is the dielectric constant of water, approximated by a temperature function, T, [34], in the form.

$$\xi = b_1\cdot(b_2 + b_3\cdot T + b_4\cdot T^2) \tag{25}$$

where b_j represents each of the adjustment coefficients.

The value of the ratio of F/ξ from Eq. (25) is very large. According to Eq. (24), any significant charge separation, $\Sigma n_j c_j$, would lead to a significant variation in the potential gradient, dφ/dx, which is unlikely. Therefore, it is common to apply the condition of electroneutrality.

$$\sum_j n_j c_j = 0 \tag{26}$$

In the case of oxygen, it is assumed that the flux density at a point of the crevice is proportional to the difference between the concentration outside the cavity, $C_{7,\text{outside the cavity}}$, and its concentration at that point, C_7. Thus, Eq. (22), is rewritten as follows:

$$\frac{\partial c_7}{\partial t} = wD_7^m\frac{\partial^2 c_7}{\partial x^2} + K_{perm}(c_{7,\text{outsidethecavity}} - c_7) \tag{27}$$

where K_{perm} is the permeability coefficient.

Eqs. (22), (24) and (27), together with the expressions of chemical reactions, constitute eight nonlinear differential equations, one for each species and the electric potential, Table 1.

In this work only the concentrations at steady state provided by the network method are of interest. Therefore, the first term of Eqs. (22) and (27) is null. Once these equations are solved, the current density of Fe^{2+} can be obtained. This is related to the corrosion rate, CR, according to Eq. (28).

$$CR = \frac{j_1\alpha_1 M_1}{n_1 F\rho_1} \tag{28}$$

where M_1 is the molecular mass of iron and ρ is the density.

The network model

The complete network model is formed by eight coupled networks, one for each species and another for the electric potential, and their boundary equations. Although the rules for designing the model are explained in González-Fernández and Alhama [16], its process is briefly described here for a better comprehension. First, we have to set the equivalence between species concentration or electrostatic potential and electric voltage, $c_j \equiv V_j$ and $\varphi \equiv V\varphi$.

Eqs. (22), (24) and (27) are developed as follows

$$-\frac{\partial c_j}{\partial t} + wD_j^m\frac{\partial^2 c_j}{\partial x^2} + wD_j^m\frac{nF}{RT}\frac{\partial c_j}{\partial x}\frac{\partial\varphi}{\partial x} + wD_j^m\frac{nF}{RT}c_j\frac{\partial^2\varphi}{\partial x^2} + wv_j = 0 \tag{29}$$

Electroneutrality conditions are:

$$-\frac{\partial c_j}{\partial t} + wD_j^m\frac{\partial^2 c_j}{\partial x^2} + wD_j^m\frac{nF}{RT}\frac{\partial c_j}{\partial x}\frac{\partial\varphi}{\partial x} + wv_j = 0 \tag{30}$$

$$\frac{\partial^2\varphi}{\partial x^2} + \frac{F}{\xi}(2c_1 + c_2 + c_3 - c_4 + c_5 - c_6) = 0 \tag{31}$$

$$-\frac{\partial c_7}{\partial t} + wD_7^m\frac{\partial^2 c_7}{\partial x^2} + K_{perm}(c_{7,\text{outsidethecavity}} - c_7) = 0 \tag{32}$$

Secondly, variable x, that is, the distance from the edge of the crevice (metal surface) until the end of cavity, is discretized in a determined number of volume elements. By means of the nomenclature of Fig. 2, Eq. (30) provides the finite-difference differential equation in steady state for species 1–6, whereas time remains as a continuous variable in the equation:

$$\underbrace{wv_j}_{I_{j,I}} + A_1\underbrace{\left[\frac{C_{j,X+\frac{\Delta X}{2}} - C_{j,X-\frac{\Delta X}{2}}}{\Delta X}\right]}_{I_{j,II}}\left[\frac{\varphi_{j,X+\frac{\Delta X}{2}} - \varphi_{j,X-\frac{\Delta X}{2}}}{\Delta X}\right] + \frac{1}{A_{j,2}}\underbrace{\left[\frac{C_{j,X+\frac{\Delta X}{2}} - C_{j,x}}{\frac{\Delta X^2}{2}}\right]}_{I_{j,in}} - \frac{1}{A_{j,2}}\underbrace{\left[\frac{C_{j,X} - C_{j,X-\frac{\Delta X}{2}}}{\frac{\Delta X^2}{2}}\right]}_{I_{j,out}} = 0 \tag{33}$$

where A_1 and $A_{j,2}$ are given:

$$A_1 = wD_j^m\frac{nF}{RT} \tag{34}$$

$$A_{j,2} = wD_j^m \tag{35}$$

Eq. (31) provides the finite-difference differential equation in steady state for electrostatic potential:

Table 1
Set of eight nonlinear differential governing equations.

Species	Equation
Fe^{2+} (species 1)	$\frac{\partial c_1}{\partial t} = wD_1^m\frac{\partial}{\partial x}\left(\frac{\partial c_1}{\partial x} + \frac{nF}{RT}c_1\frac{\partial\varphi}{\partial x}\right) + w(-K_{hy}\cdot c_1 + c_2c_5)$
$Fe(OH)^+$ (species 2)	$\frac{\partial c_2}{\partial t} = wD_2^m\frac{\partial}{\partial x}\left(\frac{\partial c_2}{\partial x} + \frac{nF}{RT}c_2\frac{\partial\varphi}{\partial x}\right) + w(K_{hy}\cdot c_1 - c_2c_5 - K_{pr}\cdot c_2 + c_5)$
Na^+ (species 3)	$\frac{\partial c_3}{\partial t} = wD_3^m\frac{\partial}{\partial x}\left(\frac{\partial c_3}{\partial x} + \frac{nF}{RT}c_3\frac{\partial\varphi}{\partial x}\right)$
Cl^- (species 4)	$\frac{\partial c_4}{\partial t} = wD_4^m\frac{\partial}{\partial x}\left(\frac{\partial c_4}{\partial x} + \frac{nF}{RT}c_4\frac{\partial\varphi}{\partial x}\right)$
H^+ (species 5)	$\frac{\partial c_5}{\partial t} = wD_5^m\frac{\partial}{\partial x}\left(\frac{\partial c_5}{\partial x} + \frac{nF}{RT}c_5\frac{\partial\varphi}{\partial x}\right) + w(K_{hy}\cdot c_1 - c_2c_5 - K_{pr}\cdot c_2 + c_5 + K_w - c_5c_6$
OH^- (species 6)	$\frac{\partial c_6}{\partial t} = wD_6^m\frac{\partial}{\partial x}\left(\frac{\partial c_6}{\partial x} + \frac{nF}{RT}c_6\frac{\partial\varphi}{\partial x}\right) + w(K_w - c_5c_6)$
O_2 (species 7)	$\frac{\partial c_7}{\partial t} = wD_7^m\frac{\partial^2 c_7}{\partial x^2} + K_{perm}(c_{7,\text{outsidethecavity}} - c_7)$
φ (Electric potential)	$\frac{\partial^2\varphi}{\partial x^2} + \frac{F}{\xi}(2c_1 + c_2 + c_3 - c_4 + c_5 - c_6) = 0$

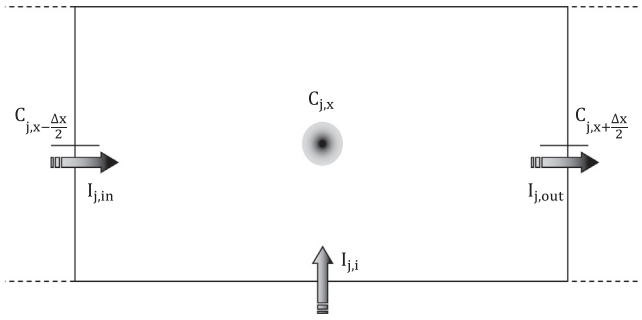

Fig. 2. Nomenclature of segments or volume elements.

$$F(2c_1 + c_2 + c_3 - c_4 + c_5 - c_6) + \frac{1}{A_{j,2}}\left[\frac{\varphi_{j,x+\frac{\Delta x}{2}} - \varphi_{j,x}}{\frac{\Delta x^2}{2}}\right] - \frac{1}{A_{j,2}}\left[\frac{\varphi_{j,x} - \varphi_{j,x-\frac{\Delta x}{2}}}{\frac{\Delta x^2}{2}}\right] = 0 \tag{36}$$

where A_{φ} is given:

$$A_{\varphi} = \xi \tag{37}$$

Equation (32) provides the finite-difference differential equation in steady state for species 7.

$$K_{perm}(c_{7,\text{outside}} - c_7) + \frac{1}{A_{7,2}}\left[\frac{c_{7,x+\frac{\Delta x}{2}} - c_{7,x}}{\frac{\Delta x^2}{2}}\right] - \frac{1}{A_{7,2}}\left[\frac{c_{7,x} - c_{7,x-\frac{\Delta x}{2}}}{\frac{\Delta x^2}{2}}\right] = 0 \tag{38}$$

where A_7 is given:

$$A_7 = wD_7^m \tag{39}$$

The addends of these equations are interpreted as electric currents which are balanced in a common node according to the current's Kirchhoff's law. The equivalence between the terms $I_{j,in}$ and $I_{j,out}$ of Eqs. (33), (36) and (38) and their equivalent electrical items is done by simple resistors, $R_{j,in}$ and $R_{j,out}$ respectively. However, the terms, $I_{j,I}$ and $I_{j,II}$, are considered as controlled current sources. Boundary conditions are implemented by batteries and controlled voltage-sources.

Fig. 3 shows the network model of a volume element for each species. Third subscript is added referring to the species, to each controlled source so as to ease its understanding.

More detailed information about the model in Sánchez-Pérez [23].

Simulation and results

Table 2 shows the values of the parameters used in the calculation of the current density for species Fe^{2+} (species 1), H^+ (species 2), OH^- (species 5) and O_2 (species 6), given by Engelhard et al. [10].

Table 3 contains the equilibrium constants of reactions (18)–(21).

The adjustment coefficients of the dielectric constant of water, Eq. (25), are: $b_1 = 10^{-9}/36\pi$, $b_2 = 249.21$, $b_3 = -0.79069$ and $b_4 = 0.00072997$. Molecular diffusion coefficients are defined in Table 4.

In their model, Engelhard et al. [10] used the current density of passivation, j_p. Therefore, to validate our model, in Eq. (1), we substitute the current density produced by the iron oxidation by the passivation current density, which is assumed to be irrespective of the electrostatic potential. The use of the passivation current density converts the material into a passive metal that is corroded very slowly.

Fig. 4 shows the relationship between the behavior of the dissolved species concentration and the distance from the edge of the crevice to a given passivation current. The values obtained for the concentration of H^+ and OH^- coincide with those obtained by Engelhard et al. [10], although small differences exist for other species. This is due to the simplification associated with the electroneutrality condition that has not been used, Eq. (26). This simplification assumes zero total charge in the potential network.

Having demonstrated the validity of the model, we next proceed to study the behavior of species concentrations in the spontaneous process, that is, in the absence of passivation current densities and other parameters. Thus, it is possible to apply the study of the different parameters to practical cases such as pitting corrosion in reinforced concrete.

To better compare the variations caused by changing parameters, Fig. 5 shows the difference between species concentrations at a point and their concentrations outside the crevice along the cavity, in the same case as that studied by Engelhard et al. [10], but in the absence of passivation current densities.

Fig. 6 shows the effect of increasing the pH, Fig. 7 the influence of increasing the temperature and Fig. 8 the effect of increasing the sodium chloride concentration outside the cavity. Fig. 9 shows the influence of increasing the oxygen concentration outside the cavity and Fig. 10 the effect of increasing the crevice depth. All these figures refer to the parameters used by Engelhard et al. [10], in the absence of passivation currents.

As may be observed, Figs. 5 and 6 show that the pH strongly affects the difference between concentrations of iron II and iron II hydroxide cations at a point, and their concentrations outside the crevice along the cavity, hereafter concentration difference. This influence is due to the effect of pH on the electrochemical reactions at the metal surface. In the same way, the pH affects the concentration difference of sodium cations. This effect is explained by the strong influence of pH on the balance of other species, through the potential network. Fig. 6 shows that the pH hardly affects the chlorine anion concentration. This influence is particularly marked for concentration difference values of this ion lower than 10^{-7} M. This phenomenon arises because this species does not react chemically, and is only influenced by the processes of diffusion and electromigration. The relationship between pH and the concentration difference of hydrogen cation is logical. At basic pH values, the variation of the difference is low because the concentration of this species is very low. In the case of hydroxyl ion species, the same effect is observed for hydrogen cations. As these ions react to form iron II hydroxide cation, this effect is further accentuated. Finally, and as expected, the pH had little influence on the variation of concentration difference of oxygen, since it only affects the processes of diffusion and permeability.

A comparison of Figs. 5 and 7 shows that a small temperature change slightly affects the concentration difference of iron II and iron II hydroxide cations. Although temperature directly influences electrochemical reactions on the metal, this effect is minimal for basic pH, and greater variation is needed to produce an appreciable effect. The same figures show that temperature also affects the concentration difference of sodium cations, an effect that is explained by the influence of temperature on the diffusion coefficients. As in the case of the concentration difference of sodium cation, temperature also affects the results of the concentration difference of chlorine anion. In this case, the variation occurs at concentration differences below 10^{-8} M. The influence of temperature on the concentration difference of hydrogen cation is low, as this parameter acts only through diffusivity coefficients and electrochemical reactions. For the latter, at basic pH the influence of temperature is even lower. In the case of the concentration difference of hydroxyl ions, temperature has the same effect as for hydrogen cations. In the same way as for the pH, the reaction of these ions to form iron II hydroxide cation is accentuated with the influence of temperature. Finally, the effect of temperature on the concentration difference of oxygen is evident. In this case, the parameter acts through diffusion and electrochemical reactions.

Moreover, a comparison of Figs. 5 and 8 shows that a large variation occurs in the concentration difference of iron II and iron II hydroxide

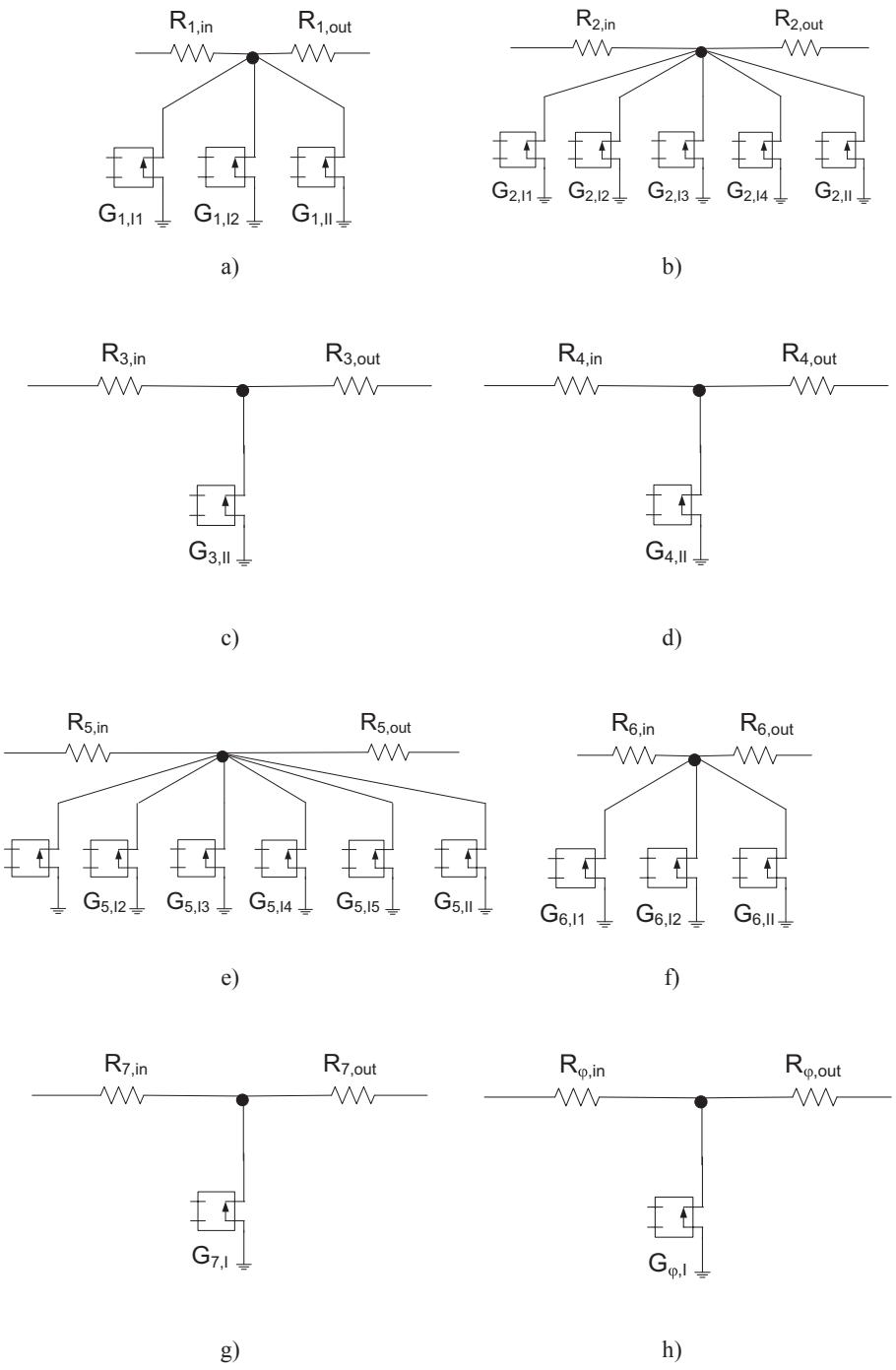

Fig. 3. Network model of a volume element: a) species 1, (b) species 2, (c) species 3, (d) species 4, (e) species 5, (f) species 6, (g) species 7 and (h) electrostatic potential.

Table 2
Electrochemical parameters for the current density of different species [5,6,10].

Species	a_1	a_2	a_3	j_{oRef}
H^+	1	0	0.5	2000 A·cm/mol
OH^-	0	0	0.5	$8.0 \cdot 10^{-8}$ A/cm^2
O_2	0	1	0.5	1620 A·cm/mol
Fe^{2+}	0	0	1	$2.7 \cdot 10^{-15}$ A/cm^2

Table 3
Equilibrium constants for chemical reactions [10].

Reaction	Hydrolysis of iron II ion	Precipitation of iron II hydroxide	Water dissociation
Units	M	M	M^2
K	$10^{-9.8}$	$10^{-4.9}$	$10^{-13.98}$

Table 4
Molecular diffusion coefficients at 20 °C [10,35–37].

Species	Molecular diffusion coefficients (cm^2/s)
Fe^{2+}	$7.2000 \cdot 10^{-6}$
$Fe(OH)^{+}$	$1.0000 \cdot 10^{-5}$
Na^{+}	$1.3340 \cdot 10^{-5}$
Cl^{-}	$2.0320 \cdot 10^{-5}$
H^{+}	$9.3020 \cdot 10^{-5}$
OH^{-}	$5.3000 \cdot 10^{-5}$
O_2	$2.2900 \cdot 10^{-5}$

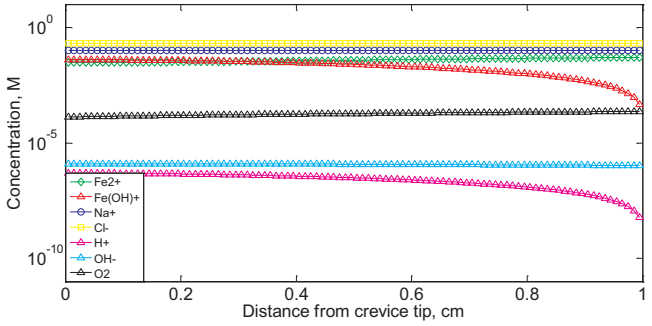

Fig. 4. Species concentrations along the cavity: temperature = 25 °C, crevice width = 0.001 m, crevice depth = 0.01 m, Oxygen concentration outside the cavity = $0.229 \cdot 10^{-3}$ mol/l, sodium chloride concentration outside the cavity = 0.1 mol/l, passivation current density: 0.1 A/m^2, permeability coefficient = $1 \cdot 10^{-6}$ cm/s and pH = 8.

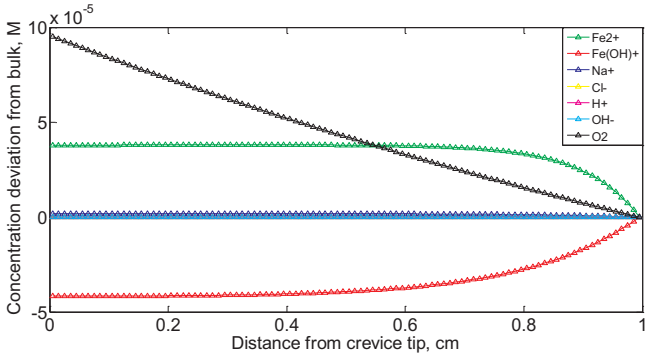

Fig. 5. Difference between species concentrations at a point and their concentrations outside the crevice along the cavity: temperature = 25 °C, crevice width = 0.001 m, crevice depth = 0.01 m, Oxygen concentration outside the cavity = $0.229 \cdot 10^{-3}$ mol/l, sodium chloride concentration outside the cavity = 0.1 mol/l, permeability coefficient = $1 \cdot 10^{-6}$ cm/s and pH = 8.

cations when the sodium chloride concentration is increased. Although this parameter does not directly affect electrochemical reactions on the metal, it does so indirectly through its effect on the potential. These same figures show that the sodium chloride concentration affects, obviously, the variation of the concentration difference of sodium cations. If the sodium chloride concentration used by Engelhard et al. [10] is increased tenfold, the concentration difference of this ion changes from 10^{-8} to 10^{-5} M, and that is due to the influence of this parameter on the potential and the concentration of this species itself. This concentration has the same effect on the concentration difference of chlorine anion as on the concentration difference of sodium cation. The concentration of sodium chloride affects the concentration difference of hydrogen cations indirectly, because it influences the potential of the electrochemical reaction of hydrogen cation. The concentration of sodium chloride in the case of concentration difference of hydroxyl ions produces the same effect as the concentration difference of hydrogen cations. As it is the case with the pH, the reaction of these ions to form

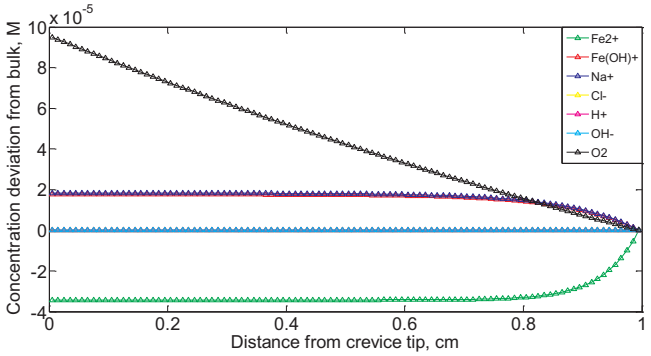

Fig. 6. Difference between species concentrations at a point and their concentrations outside the crevice along the cavity: temperature = 25 °C, crevice width = 0.001 m, crevice depth = 0.01 m, Oxygen concentration outside the cavity = $0.229 \cdot 10^{-3}$ mol/l, sodium chloride concentration outside the cavity = 0.1 mol/l, permeability coefficient = $1 \cdot 10^{-6}$ cm/s and pH = 9.

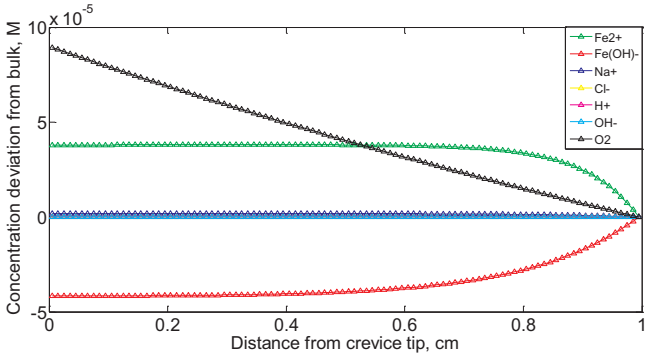

Fig. 7. Difference between species concentrations at a point and their concentrations outside the crevice along the cavity: temperature = 30 °C, crevice width = 0.001 m, crevice depth = 0.01 m, Oxygen concentration outside the cavity = $0.229 \cdot 10^{-3}$ mol/l, sodium chloride concentration outside the cavity = 0.1 mol/l, permeability coefficient = $1 \cdot 10^{-6}$ cm/s and pH = 8.

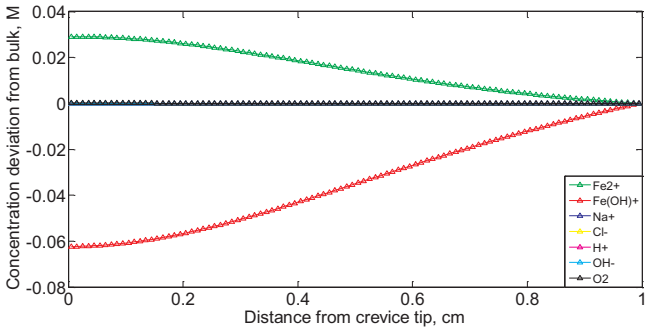

Fig. 8. Difference between species concentrations at a point and their concentrations outside the crevice along the cavity: temperature = 25 °C, crevice width = 0.001 m, crevice depth = 0.01 m, Oxygen concentration outside the cavity = $0.229 \cdot 10^{-3}$ mol/l, sodium chloride concentration outside the cavity = 1 mol/l, permeability coefficient = $1 \cdot 10^{-6}$ cm/s and pH = 8.

iron II hydroxide cation accentuates the effect of this parameter. Finally, the effect of sodium chloride concentration on the concentration difference of oxygen occurs indirectly, because it affects the potential of the electrochemical reaction of oxygen.

Furthermore, Figs. 5 and 9 show that a small increase in the oxygen concentration causes a large variation in the concentration difference of iron II and iron II hydroxide cations, an effect due to the direct influence of this concentration on the electrochemical reactions. Similarly, the same figures illustrate the low influence of oxygen concentration on

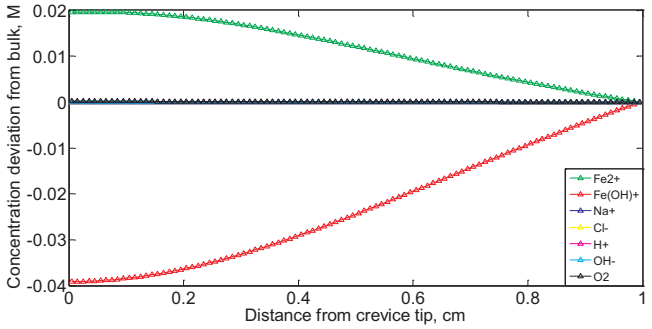

Fig. 9. Difference between species concentrations at a point and their concentrations outside the crevice along the cavity: temperature = 25 °C, crevice width = 0.001 m, crevice depth = 0.01 m, Oxygen concentration outside the cavity = $0.458 \cdot 10^{-3}$ mol/l, sodium chloride concentration outside the cavity = 0.1 mol/l, permeability coefficient = $1 \cdot 10^{-6}$ cm/s and pH = 8.

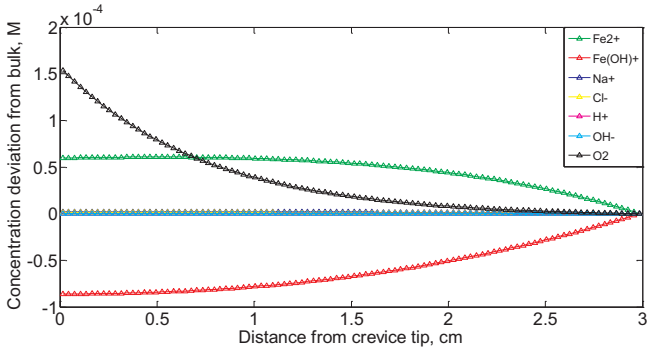

Fig. 10. Difference between species concentrations at a point and their concentrations outside the crevice along the cavity: temperature = 25 °C, crevice width = 0.001 m, crevice depth = 0.03 m, Oxygen concentration outside the cavity = $0.229 \cdot 10^{-3}$ mol/l, sodium chloride concentration outside the cavity = 0.1 mol/l, permeability coefficient = $1 \cdot 10^{-6}$ cm/s and pH = 8.

the concentration difference of species which do not participate in electrochemical reactions: the sodium cations and chlorine anions. The effect of oxygen concentration on the concentration difference of hydrogen cation is due to the effect this concentration has on electrochemical reactions. The effect of oxygen concentration on the concentration difference of hydroxyl ion is the same as the concentration difference of hydrogen cation. Similarly to pH, the reaction of these ions to form iron II hydroxide cation accentuates the effect of this concentration.

Finally, a comparison of Figs. 5 and 10 shows that the crevice depth has a slight effect on all the species. This effect, coupled with diffusion phenomena, reflects the higher concentration gradients near the edge of the crevice, meaning that below a certain depth its influence is reduced.

Since the concentrations of iron II and iron II hydroxide cations are closely related to the corrosion rate, we study only the distribution of these variables in the crevice. Figs. 11–15 show the distribution of selected species for two values of a given parameter.

Fig. 11 shows the effect of pH on concentrations of certain cations in the cavity. The concentration of these cations decreases with increasing pH due to the inverse relationship between pH and the rate of electrochemical reactions. Throughout the cavity, this relation is maintained.

The effect of temperature on a selection of cations is studied in Figs. 12a–12c. At the deepest point of the crevice, it can be observed that the concentration of iron II hydroxide cation increases slightly with increasing temperature, while in the case of the iron II cation the influence is hardly noticeable. These results can be explained by the temperature effect on the current density at the deepest point of the crevice. In the cavity, the temperature's influence on concentrations tends to increase with depth. This effect is due to the boundary conditions at the opposite point of the metal surface (outside the cavity), which depend on equilibrium concentrations, which, in our model, are not a function of the temperature, since the experimental data given by Engelhard et al. [10] are irrespective of this parameter, Table 3.

Fig. 13 shows the effect of sodium chloride concentration of selected cations. At the deepest point of the crevice, the concentration of iron II cations decreases with increasing sodium chloride concentration. In the cavity, the effect of this concentration increases with depth. This influence can be explained by the boundary conditions and the electromigration that occurs in the domain. Thus, the boundary condition at the deepest point of the crevice depends on its equilibrium concentration, which is not influenced by the sodium chloride concentration. In addition, the boundary condition at the deepest point of the crevice depends on the gradient of the ion concentration studied, which, in turn, depends on the current density of the electrochemical reaction that is irrespective of the sodium chloride concentration. In the domain, concentration gradients depend on electromigration, which is affected by the sodium chloride concentration and chemical reactions between both cations. At the deepest point of the crevice, the concentration of iron II hydroxide cations increases with the sodium chloride concentration. In the cavity, the effect of this concentration increases with depth. The explanation is the same as that given for another cation, iron II. From Fig. 13 it can also be seen that the sum of both cations concentrations, which is related to the corrosion rate, increases with the sodium chloride concentration. As stated in the bibliography, an increase in the sodium chloride concentration produces an increase in corrosion [38].

The effect of oxygen concentration on selected cations is shown in Fig. 14. At the deepest point of the crevice, the concentration of iron II cations decreases with increasing oxygen concentration. In the cavity, the influence of this concentration increases with depth. This effect can be explained taking into account the boundary conditions and the potential at the deepest point of the crevice (metal surface). Thus, the boundary condition at the opposite point of the metal surface (outside the cavity) depends on its equilibrium concentration, which is not influenced by oxygen concentration. In addition, the boundary condition at the deepest point of the crevice depends on the concentration ion gradient, which, in turn, is influenced by the current density of the electrochemical reaction that is dependent only on the oxygen concentration for the iron II cation. In the domain, concentration gradients are dependent on the potential, which, in turn, depends on the oxygen concentration. At the deepest point of the crevice, the concentration of iron II hydroxide cations increases with oxygen concentration. In the cavity, the effect of this concentration increases with depth. The explanation is the same as for the iron II cation. As expected, in Fig. 14 the

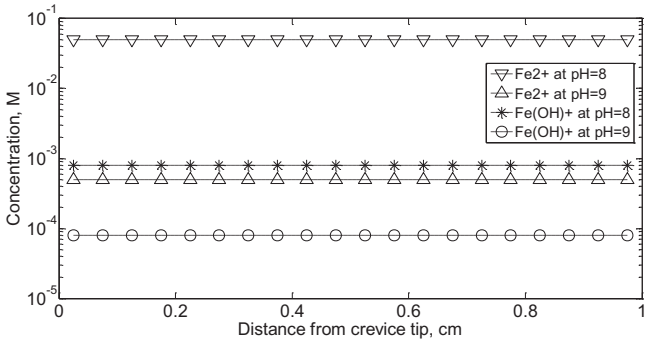

Fig. 11. Concentration of iron II and iron II hydroxide cations along the cavity: temperature = 25 °C, crevice width = 0.001 m, crevice depth = 0.01 m, Oxygen concentration outside the cavity = $0.229 \cdot 10^{-3}$ mol/l, sodium chloride concentration outside the cavity = 0.1 mol/l and permeability coefficient = $1 \cdot 10^{-6}$ cm/s.

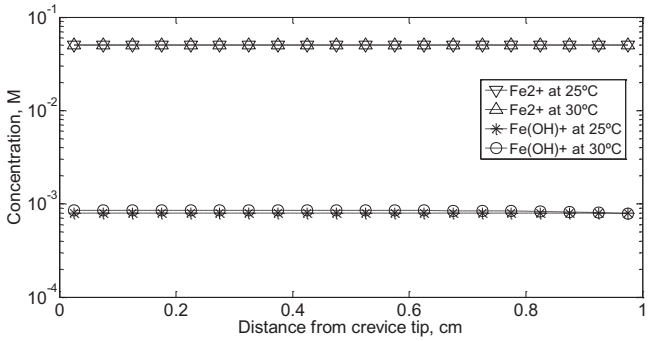

Fig. 12a. Concentration of iron II and iron II hydroxide cations along the cavity: crevice width = 0.001 m, crevice depth = 0.01 m, Oxygen concentration outside the cavity = $0.229 \cdot 10^{-3}$ mol/l, sodium chloride concentration outside the cavity = 0.1 mol/l, permeability coefficient = $1 \cdot 10^{-6}$ cm/s and pH = 8.

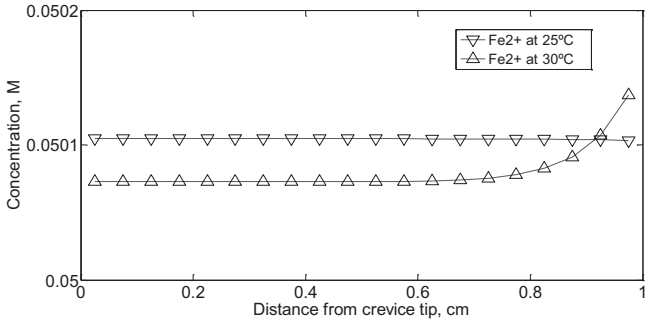

Fig. 12b. Concentration of iron II cation along the cavity: crevice width = 0.001 m, crevice width = 0.01 m, Oxygen concentration outside the cavity = $0.229 \cdot 10^{-3}$ mol/l, sodium chloride concentration outside the cavity = 0.1 mol/l, permeability coefficient = $1 \cdot 10^{-6}$ cm/s and pH = 8.

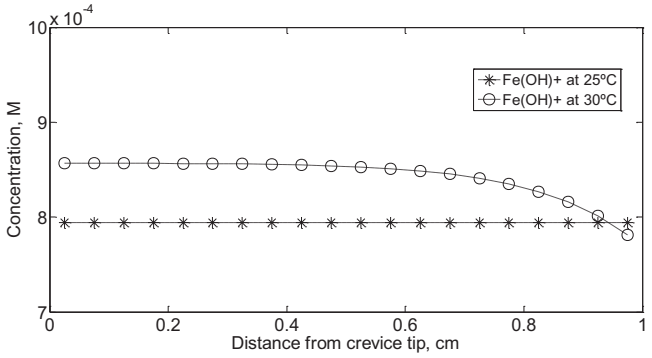

Fig. 12c. Concentration of iron II hydroxide cation along the cavity: crevice width = 0.001 m, crevice depth = 0.01 m, Oxygen concentration outside the cavity = $0.229 \cdot 10^{-3}$ mol/l, sodium chloride concentration outside the cavity = 0.1 mol/l, permeability coefficient = $1 \cdot 10^{-6}$ cm/s and pH = 8.

sum of both cation concentrations, which is related to the corrosion rate, increases with the oxygen concentration.

Figs. 15a–15c show the effect of the crevice depth on selected cations. A comparative study of this parameter's influence does not make sense, given the large change in the curve shape when it varies.

Finally, the corrosion rates as a function of several parameters are depicted in Figs. 16 and 17. Fig. 16 shows corrosion rates as a function of the pH and temperature. The graph has been rotated about the vertical axis to better appreciate the slope of surfaces. As can be seen, an increase in corrosion rate occurs as the pH decreases. As for the temperature's effect, a slight increase in corrosion is evident as temperature increases.

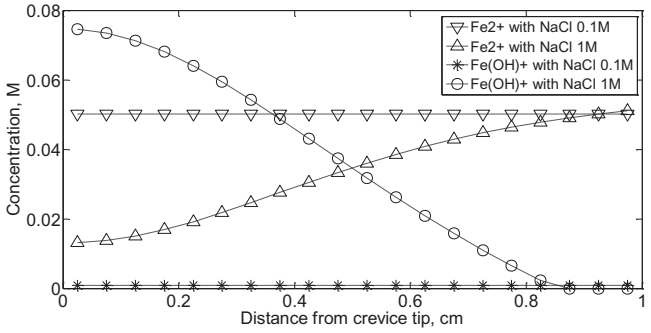

Fig. 13. Concentration of iron II and iron II hydroxide cations along the cavity: temperature = 25 °C, crevice width = 0.001 m, crevice depth = 0.01 m, Oxygen concentration outside the cavity = $0.229 \cdot 10^{-3}$ mol/l, permeability coefficient = $1 \cdot 10^{-6}$ cm/s and pH = 8.

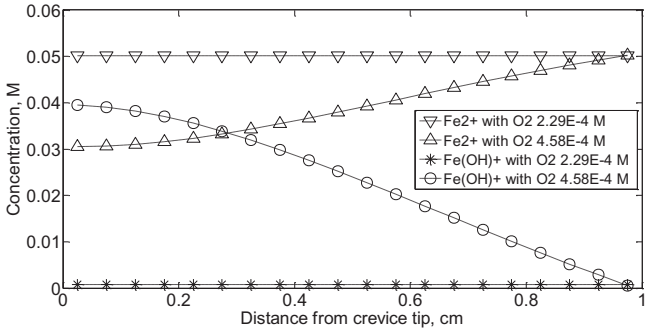

Fig. 14. Concentration of iron II and iron II hydroxide cations along the cavity: temperature = 25 °C, crevice width = 0.001 m, crevice depth = 0.01 m, sodium chloride concentration outside the cavity = 0.1 mol/l, permeability coefficient = $1 \cdot 10^{-6}$ cm/s and pH = 8.

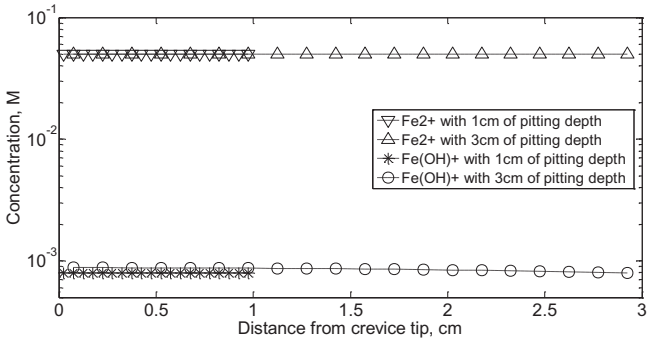

Fig. 15a. Concentration of iron II and iron II hydroxide cations along the cavity: temperature = 25 °C, crevice width = 0.001 m, Oxygen concentration outside the cavity = $0.229 \cdot 10^{-3}$ mol/l, sodium chloride concentration outside the cavity = 0.1 mol/l, permeability coefficient = $1 \cdot 10^{-6}$ cm/s and pH = 8.

Fig. 17 shows corrosion rates as a function of the pH and oxygen concentration. This graph has been rotated about the vertical axis to better appreciate the slope of surfaces. As can be seen an increase in corrosion rate occurs with decreasing pH. As for the effect of oxygen concentration, corrosion increases as the value of this parameter increases.

If Figs. 16 and 17 are compared, the corrosion rate at basic pH values can be seen to mainly depend on the oxygen concentration.

Applications in the engineering context

In this section we will demonstrate the different applications that our study would have in the solution of problems arising in different

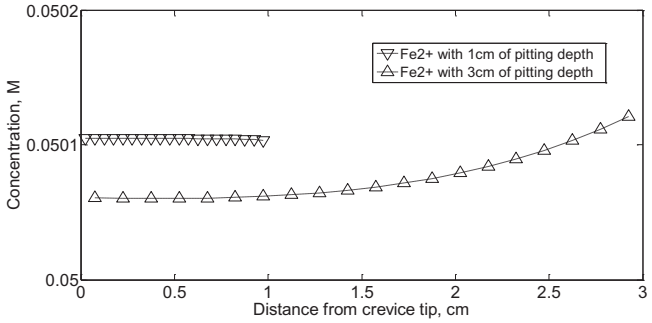

Fig. 15b. Concentration of iron II cation along the cavity: temperature = 25 °C, crevice width = 0.001 m, Oxygen concentration outside the cavity = $0.229 \cdot 10^{-3}$ mol/l, sodium chloride concentration outside the cavity = 0.1 mol/l, permeability coefficient = $1 \cdot 10^{-6}$ cm/s and pH = 8.

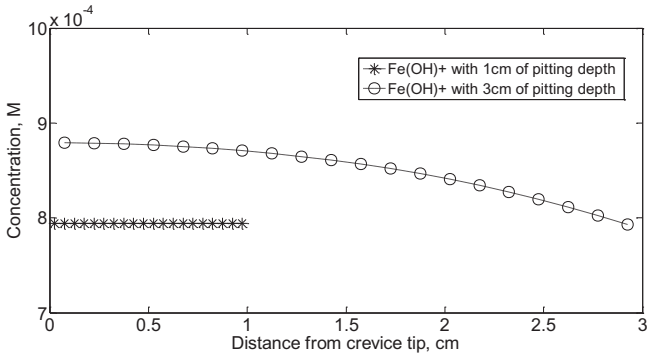

Fig. 15c. Concentration of iron II hydroxide cation along the cavity: temperature = 25 °C, crevice width = 0.001 m, Oxygen concentration outside the cavity = $0.229 \cdot 10^{-3}$ mol/l, sodium chloride concentration outside the cavity = 0.1 mol/l, permeability coefficient = $1 \cdot 10^{-6}$ cm/s and pH = 8.

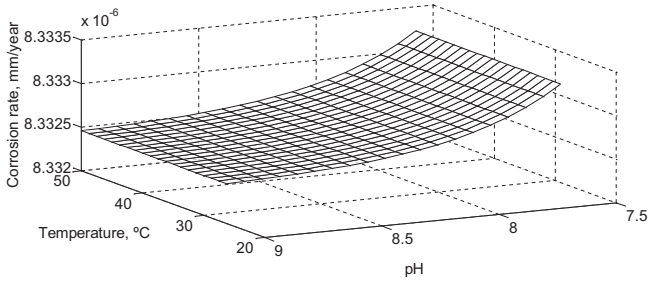

Fig. 16. Predicted corrosion rate: crevice width = 0.001 m, crevice depth = 0.01 m, Oxygen concentration outside the cavity = $0.229 \cdot 10^{-3}$ mol/l, sodium chloride concentration outside the cavity = 0.1 mol/l and permeability coefficient = $1 \cdot 10^{-6}$ cm/s.

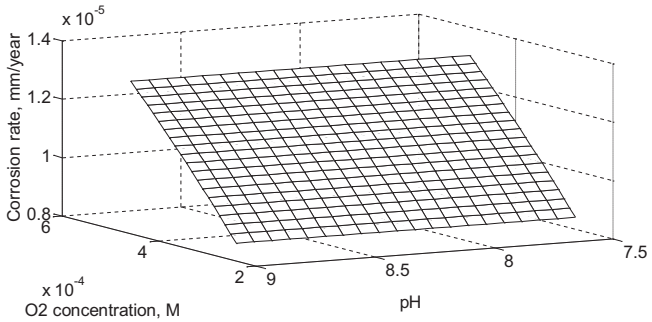

Fig. 17. Predicted corrosion rate: temperature = 25 °C, crevice width = 0.001 m, crevice depth = 0.01 m, sodium chloride concentration outside the cavity = 0.1 mol/l and permeability coefficient = $1 \cdot 10^{-6}$ cm/s.

fields of engineering:

Pitting corrosion in reinforced concrete

If we apply the study of the parameters above to pitting corrosion in reinforced concrete, we can observe that the parameters to control are pH and oxygen, and sodium chloride concentration, since there is a direct relationship between oxygen and sodium chloride concentration, and the increase in corrosion. However, this relationship is inversely proportional to pH. If we look at Fig. 13, an increase of ten times the concentration of chloride ions leads to an increase of approximately nine times the total concentration of iron cations. This effect is confirmed in the bibliography, since with the presence of chlorides, pitting corrosion occurs, because the passive layer on small areas of the surface is lost. Chloride ions act as a catalyst within the cavity and accelerate the corrosion [15,39]. In this way, it is necessary to control the concentration of chlorides in structures exposed to marine environments or submerged in seawater, since otherwise these structures would considerably reduce their useful life. If we take the relationship obtained from Fig. 13, an increase of twice as much chloride concentration could halve its useful life.

On the other hand, from Figs. 14 and 17, it can be deduced that an increase of twice the oxygen concentration leads to an increase of approximately 1.5 times in the corrosion rate. In this way, both parameters, chloride and oxygen, must be controlled for this type of structures since they considerably shorten their useful life.

Pitting corrosion on buried pipes

As in the previous case, the important parameters are chlorine ions, oxygen and pH. In this case, one of the most important parameters to control is the oxygen concentration since the rest of them have legislative limits, Council Directive 98/83/EC [40]. Chloride ions concentration and pH also have to be studied since in the values range allowed by the legislation corrosion could be accelerated. Thus, in the case of chloride ions, a maximum value of 250 mg/l (0.0071 M) of chloride concentration is established, which implies a fairly low concentration value. If we observe the values obtained from Fig. 13, we find a concentration approximately ten times lower than the one studied, which would be equivalent to a concentration of iron cations nine times lower. Therefore, this maximum value, which was established for the protection of the population's health, has indirectly served to protect the metallic conduits of drinking water.

For the pH parameter, the legislation establishes a range between 6.5 and 9.5. If we study Figs. 11, 16 and 17, it can be seen that for the ranges established in the legislation there is no substantial increase in corrosion when the pH decreases.

Regarding the concentration of oxygen, since this legislation does not establish a maximum value, it must be a parameter to be controlled, as a double increase in concentration implies a 1.5 times increase in the iron cations concentration.

Ship hull corrosion

In this case, the most important parameter is the chloride ion concentration since the most common range of sea salinity is between 30 and 40 psu (0.85 and 1.13 M) [41]. In this case, in Fig. 13, it can be observed that there would be a significant increase in the iron cations concentration, and therefore corrosion. Moreover, if we compare these values with those of the drinking water studied previously, it would reveal an increase in the concentration of these cations of more than ninety times.

Conclusions

The model designed successfully simulates the pitting corrosion that

occurs in a medium with basic pH. The effect on the variation of parameter values in all the concentrations of species and on their differences with their concentrations outside the crevice and along the cavity is studied for a wide range of them. Moreover, the issue of which parameter has a greater influence on the system is argued. No simplifications have been considered, although the model is firmly coupled and is susceptible to any variation of the parameters above. A comparison of the results with data published in the scientific literature for domains that establish the most complex and complete scenarios, confirms the reliability of the model. In conclusion, it can be observed that there is a direct relationship between the oxygen and sodium chloride concentration and the increase in corrosion. However, this relationship is inversely proportional to pH. These relationships have practical applications for corrosion prevention in reinforced concrete, in buried pipes and on ship hulls, among others.

Competing interests

The authors declare that they have no competing interests.

Authors' contributions

J.F. Sánchez-Pérez came up with the initial idea for the work. All authors performed the simulations and all the data analysis. All authors participated in the writing and revising of the manuscript.

References

[1] Marcus P. Introduction to the fundamentals of corrosion. In: ASM handbook, vol. 13A. ASM International; 2003. p. 3.
[2] Schweitzer PA. Corrosion mechanisms. Corrosion engineering handbook. CRC Press; 2007. p. 24.
[3] Thompson NG. Appendix E – Gas and Liquid Transmission Pipelines. CC Technologies Laboratories, Inc., Dublin, Ohio. [on line]. (quoted 2011) Available on World Wide Web: http://www.corrosioncost.com.
[4] Hebert K, Alkire R. Dissolved metal species mechanism for initiation of crevice corrosion of Aluminum: II. Mathematical model. J Electrochem Soc 1983;130:1007.
[5] Sharland SM, Tasker PW. A mathematical model of crevice and pitting corrosion I. The physical model. Corros Sci 1988;28(6):603.
[6] Sharland SM. A mathematical model of crevice and pitting corrosion II. The mathematical solution. Corros Sci 1988;28(6):621.
[7] White SP, Weira GJ, Laycock NJ. Calculating chemical concentrations during the initiation of crevice corrosion. Corros Sci 2000;42:605–29.
[8] Hebert K, Alkire R. Dissolved metal species mechanism for Initiation of crevice corrosion of aluminum II. Mathematical model. J Electrochem Soc 1983;130(5):1007–14.
[9] Williams DE, Westcott C, Fleischmann M. Stochastic models of pitting corrosion of stainless steels: I. Modeling of the initiation and growth of pits at constant potential. J Electrochem Soc 1985;132(8):1796–804.
[10] Engelhard GR, McMillion LG, Macdonald DD. A mathematical model for crevice corrosion under porous deposits. J Nucl Mater 2008;379:48–53.
[11] Walton JC. Mathematical modeling of mass transport and chemical reaction in crevice and pitting corrosion. Corros Sci 1990;30(8/9):915.
[12] Alkire RC, Lott SE. J Electrochem Soc 1989;136(11):3256–62.
[13] Alkire RC, Siitari D. Initiation of crevice corrosion: II. Mathematical model for aluminum in sodium chloride solutions. J Electrochem Soc 1982;129(3):488–96.
[14] Evitts RW. Modelling of crevice corrosion. University of Saskatchewn, Department of Chemical Engineering; 1997.
[15] Bermúdez Odriozola MA. Corrosión de las armaduras del hormigón armado en ambiente marino: zona de carrera de mareas y zona sumergida PhD Thesis Spain: Universidad Politécnica de Madrid; 2007
[16] González-Fernández CF, Alhama F, Horno J, editors. Transworld, heat transfer and the network simulation method, Research Network, Trivandrum; 2001.
[17] Kreith F. The CRC handbook of thermal engineering. CRC Press; 2000.
[18] Mills AF. Heat transfer. 2nd ed. Prentice Hall; 1998.
[19] Microsim Corporation Fairbanks, PSPICE 6.0. Irvine, California 92718; 1994.
[20] NgSpice software [on line]. (quoted 2018) Available on World Wide Web: http://ngspice.sourceforge.net/index.html.
[21] Nagel LW. SPICE (Simulation program with integrated circuit emphasis). Berkeley, CA: University of California, Electronics Res. Lab., ERL-M382; 1977.
[22] Sánchez-Pérez JF, Alhama F, Moreno JA. An efficient and reliable model based on network method to simulate CO_2 corrosion with protective iron carbonate films. Comput Chem Eng 2012;39:57–64.
[23] Sánchez-Pérez JF. Solución numérica de problemas de oxidación mediante el método de simulación por redes PhD Thesis Spain: Universidad Politécnica de Cartagena; 2012
[24] Sánchez-Pérez JF, Alhama F, Moreno JA. Numerical simulation of oxygen diffusion problems with moving oxidation fronts by network method. International Review of Chemical Engineering (I.RE.CH.E.), vol. 4(6). In: 4th International Conference on Chemical Engineering and Advanced Materials (CEAM) VIRTUAL FORUM; 2012.
[25] Sánchez-Pérez JF, Moreno JA, Alhama F. Numerical simulation of high-temperature oxidation of lubricants using the network method. Chem Eng Commun 2015;202:982–91.
[26] González-Fernández CF, Alhama F, López-Sánchez JF. Application of the network method to heat conduction processes with polynomial and potential-exponentially varying thermal properties. Numer Heat Transf A, Appl 1998;33:549.
[27] Horno J, González-Fernández CF, Hayas A. The network method for solutions of oscillating reaction-diffusion systems. J Comp Phys 1995;118:310.
[28] Soto Meca A, Alhama F, González-Fernández CF. An efficient model for solving density driven groundwater flow problems based on the network simulation method. J Hydrol 2007;339:39.
[29] Zueco J, Alhama F. Inverse estimation of temperature dependent emissivity of solid metals. J Quant Spectrosc Radiat Transf 2006;101:73.
[30] Cánovas M, Alhama I, Trigueros E, Alhama F. Numerical simulation of Nusselt-Rayleigh correlation in Bénard cells. A solution based on the network simulation method. Int J Numer Meth Heat Fluid Flow 2015;25(5):986–97.
[31] Costa JM. Fundamentos de electrodica – Cinética electroquímica y sus aplicaciones. Editorial Alhambra S.A; 1981.
[32] Handbook, A. S. M. vol. 13A. Metals Park (OH): ASM International; 2003. p. 814–50.
[33] Nesic S, Nordsveen M, Nyborg R, Stangeland A. A mechanistic model for CO2 corrosion with protective iron carbonate films. Corrosion 2001, paper no. 1040 (Houston, TX: NACE); 2001.
[34] Lide DR. Handbook of chemistry and physics 1913–1995. London, Tokyo: CRC Press; 1995.
[35] Newman JS. Electrochemical systems. 2nd ed. Englewood Cliffs, NJ: Prentice Hall; 1991.
[36] Perry RH, Green D. Perry's chemical engineers' handbook. 50th ed. New York, NY: McGraw-Hill; 1984.
[37] Kvarekvål J. A kinetic model for calculating concentration profiles and fluxes of CO2-related species across the nernst diffusion layer. Corrosion/97, 5, Houston, TX: NACE; 1997.
[38] García E, Uruchurtu J, Genescá J. Efecto de los componentes del agua de mar durante el fenómeno de corrosión por picaduras del cobre. Rev Metal Madrid 1995;31:307.
[39] Climent MA, de Vera Guillem, López JF, Viqueira E, Andrade C. A test method for measuring chloride diffusion coefficients through nonsaturated concrete. Part I. The instantaneous plane source diffusion case. Cem Concr Res 2002;32:1113–23.
[40] Council Directive 98/83/EC of 3 November 1998 on the quality of water intended for human consumption.
[41] Gobierno de España, Ministerio de Fomento, Puertos del Estado. Madrid, España. [on line]. (quoted 2016) Available on World Wide Web: http://www.puertos.es/es-es/oceanografia/Paginas/portus.aspx.